The Multi-Messenger Astrophysics of the Galactic Centre
Proceedings IAU Symposium No. 322, 2016
R.M. Crocker, S.N. Longmore & G.V. Bicknell, eds.

doi:10.1017/S174392131601259X

Status of GRMHD simulations and radiative models of Sgr A*

Monika Mościbrodzka

Department of Astrophysics/IMAPP, Radboud University,
P.O. Box 9010, 6500 GL, Nijmegen, the Netherlands
email: m.moscibrodzka@astro.ru.nl

Abstract. The Galactic center is a perfect laboratory for testing various theoretical models of accretion flows onto a supermassive black hole. Here, I review general relativistic magnetohydrodynamic simulations that were used to model emission from the central object - Sgr A*. These models predict dynamical and radiative properties of hot, magnetized, thick accretion disks with jets around a Kerr black hole. Models are compared to radio-VLBI, mm-VLBI, NIR, and X-ray observations of Sgr A*. I present the recent constrains on the free parameters of the model such as accretion rate onto the black hole, the black hole angular momentum, and orientation of the system with respect to our line of sight.

1. Introduction

The radio emission of Sgr A* has been proposed to be produced either by an advection dominated accretion flow (ADAF) onto supermassive black hole (Ichimaru 1977; Narayan *et al.* 1998; Quataert & Narayan 1999; Özel *et al.* 2000) or by a magnetized jet associated with it (Falcke *et al.* 1993; Falcke & Markoff 2000; Markoff *et al.* 2007; Yuan *et al.* 2002). Sgr A* black hole accretes at relatively low rates compared to typical Active Galactic Nuclei ($\dot{M} \approx 10^{-9} - 10^{-7}\,\mathrm{M_\odot\,yr^{-1}}$, e.g. Marrone *et al.* 2007). Consequently any ADAF or jet emission will have small angular size on the sky (from 50 to 200 microarcseconds between $\lambda = 7$ and 1 mm, Mościbrodzka *et al.* 2014). In addition, the intrinsic shape of Sgr A* is distorted by the scattering of radio waves by the free electrons in the interstellar medium (e.g. Bower *et al.* 2014). Hence, it is difficult to distinguish the models mentioned above, or rule out one of them. It is therefore a good idea to improve the models and examine what comes out from them naturally. The models of ADAFs and jets have advanced from simple semi-analytical models to fully three dimensional general relativistic magnetohydrodynamical (GRMHD) simulations. Further, the development of general relativistic radiative transfer models allowed us to compare the simulations, in various ways, to the existing multi-wavelength observational data of Sgr A*. In this paper, I review all the recent GRMHD models that have been explored in the context of Sgr A* and what we have learned by comparing them to observations.

2. Simulations of SANEs and MADs

In these models, the simulations follow the evolution of plasma and magnetic fields around Kerr black hole. The numerical models are adiabatic, i.e., the energy loss and gain occur only through adiabatic (de)compressions. As confirmed by Dibi *et al.* (2012), Drappeau *et al.* (2013) and Sadowski *et al.* (2016), skipping the radiation evolution in Sgr A* models is a good approximation. The non-radiative simulations usually start with plasma around the black hole configured into a torus structure. The initial conditions for

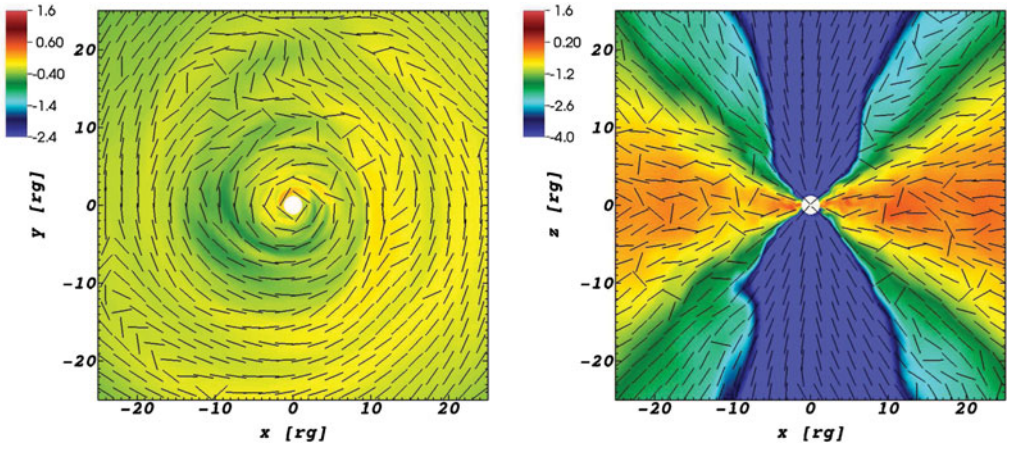

Figure 1. The evolved state of 3-D GRMHD simulation of SANE accretion flow model onto a spinning black hole. Left and right panels show log of rest-mass density in x-y plane at z=0 (equatorial plane of the disk) and x-z plane at y=0 (a cut along the black hole axis), respectively. The black ticks follow the local direction of magnetic field lines.

the plasma configuration are based on analytical solutions of thick accretion disks (for a review of thick accretion disks, see Abramowicz & Fragile 2013 and references therein). The free parameters of the numerical models are: the size of the torus, the spin of the black hole (a_*) and the initial geometry of magnetic fields.

The exact transport mechanism of the magnetic fields from large scales towards the black hole horizon is still under debate. Moreover, the exact structure of magnetic fields located far away (around the Bondi radius) from a black hole is also unconstrained. Hence, for a simplicity, simulations often start with the poloidal field lines embedded in a torus close to a black hole. The magnetic fields are sub-thermal (i.e., the gas pressure is larger than the magnetic field pressure, $\beta = P_{\rm gas}/P_{\rm mag} > 1$); the source of viscosity in the accretion disks is turbulence that arises from the magneto-rotational instability (Balbus & Hawley 1998). The choice of the initial magnetic field topology (dipole, quadrupole, or multipole) controls the development and properties of the jets (Beckwith *et al.* 2008). Steady jets tend to be produced only when an initial single loop scenario is assumed. Steady jets have two components: a magnetized, force-free spine (or jet funnel) and a jet sheath (funnel wall) surrounding it.

Two families of accretion flow models with steady jets are currently under investigation in the context of Sgr A*. First family is so-called standard and normal evolution (SANE) models in which the magnetic fields in the accretion disk are sub-thermal and turbulent, and the amount of coherent large scale magnetic field flux accumulated near horizon is relatively small (McKinney & Gammie 2004). The second group are the magnetically arrested disks (MADs) in which the disk magnetic fields are stronger, and the total flux accumulated near the black hole is at its maximum saturation level (Narayan *et al.* 2003; McKinney *et al.* 2012). The jets produced by MAD allows for the extremely efficient extraction of rotational energy from the black hole ($\eta = P_j/\dot{M}c^2 = 140\,\%$, Tchekhovskoy *et al.* 2011). Also in MADs, the strong magnetic fields can lead to a development of magnetic barrier that interrupts the accretion onto the black hole which, in turn, may appear as a significant fluctuation in light curves. Notice that larger variations in light curves may also be produced by SANE disks in which their angular momentum vectors are misaligned with that of a black hole spin. This causes the formation of plunging streams (Fragile *et al.* 2007). An excellent comprehensive review of SANEs and MADs is

https://doi.org/10.1017/S174392131601259X Published online by Cambridge University Press

given in Yuan & Narayan (2014) (in their Section 3). An example of the SANE, turbulent solution with a jet is given in Fig. 1.

3. Electron temperatures in GRMHD simulations and emission models

Emission models require providing the electron temperatures ($T_{\rm e}$) which are not evolved in the simulations discussed here. We expect that the electrons and protons in plasma around Sgr A* are thermally decoupled because of: inefficient Coulomb collisions between protons and electrons; different heat conductivities; different cooling processes; different fractions of viscous heating (energy dissipated in the MHD turbulence). The last is controlled by local plasma instabilities that are not resolved in global GRMHD simulations of accretion disks.

To account for the unresolved electron physics in GRMHD simulations, most of the earlier calculations of the radiation produced in GRMHD simulations had assumed a simple parameterization of electron temperatures, i.e., a constant $T_{\rm p}/T_{\rm e}$ ratio (Mościbrodzka *et al.* 2009). The exact value of $T_{\rm p}/T_{\rm e}$ ratio was derived by fitting the models to the observed flux and the size of Sgr A*. Early studies indicated that a best fit value is $T_{\rm p}/T_{\rm e} \approx 3$, which was later often used. However, it is likely that the true proton-to-electron temperature ratio deviates from a constant value. For example, we have recently found that the radiative properties of GRMHD models, in which $T_{\rm p}/T_{\rm e}$ is a function of local plasma magnetization, naturally reproduce the slightly inverted radio spectrum and the observed size-wavelength relation of Sgr A* (Mościbrodzka & Falcke 2013; Mościbrodzka *et al.* 2014).

More recent and detailed calculations of electron temperatures have been presented by Ressler *et al.* (2015) and Sadowski *et al.* (2016) (see also Shcherbakov *et al.* 2012). Authors evolve separate entropy equations for electron and protons including thermal conductivity and particles heating (Ressler et al. 2015) or particle heating, radiative cooling, and Coulomb couplings (Sadowski *et al.* 2016). It is found that thermal conductivity does not have a significant effect on the electron temperatures, at least for the magnetic field configuration setup adopted by the authors. The most significant effect on electron temperatures is imposed by a model of plasma heating. This heating model is adopted from a model for the solar wind (Howes 2011) that results in a proton to electron temperature ratio depending on the local plasma magnetization. The relationship that roughly reflects this physics is

$$\frac{T_p}{T_e} = R_{\rm low}\frac{1}{1+\beta^2} + R_{\rm high}\frac{\beta^2}{1+\beta^2} \tag{3.1}$$

where $R_{\rm high}$ and $R_{\rm low}$ are free parameters. Here we assume that $T_e < T_p$ and compute the proton temperature using the GRMHD simulation data. All advanced electron and proton temperature models are based on SANE models. The temperatures of electrons in strongly magnetized MAD models are uncertain. However if one needs to fit the Sgr A* spectrum with a MAD model, an extremely high $T_{\rm p}/T_{\rm e} \sim 1000$ has to be assumed in the strongly magnetized disk (see next section). This seems to be in contradiction with the findings of Ressler *et al.* (2015).

GRMHD simulations with assumed electron physics are coupled to radiative transfer codes to produce radio images of the simulation or broadband spectrum of the GRMHD models. Example images of a SANE model from Mościbrodzka *et al.* (2014) and Fraga-Encinas *et al.* (2016) are shown in Fig.2. The electron temperature here is computed using Eq. 3.1 with $R_{\rm high} = 20$ and $R_{\rm low} = 1$ (where $R_{\rm high/low}$ are chosen based on

https://doi.org/10.1017/S174392131601259X Published online by Cambridge University Press

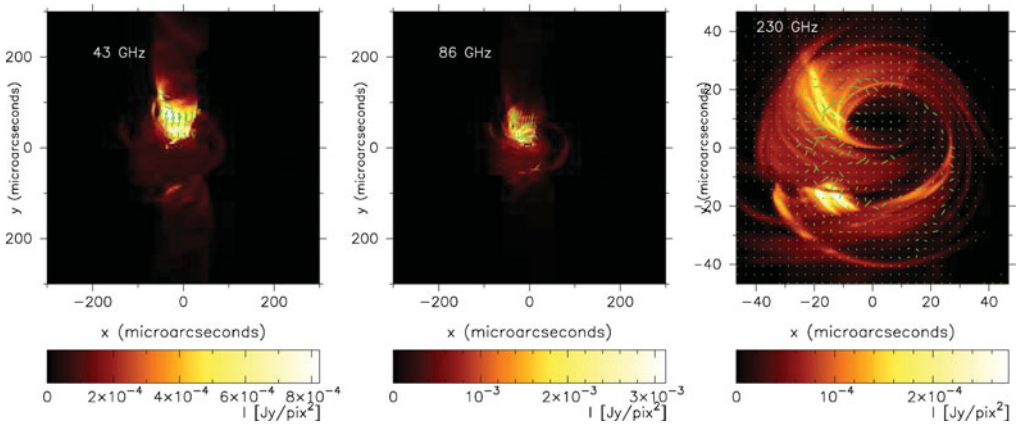

Figure 2. Each panel displays model radio images (synchrotron emission maps) of a 3D GRMHD simulation of SANE disk with a jet. Left, middle, and right columns show the model appearance at λ=7, 3.5, and 1.3mm, respectively. Color intensity codes the radiation intensity in linear scale. The direction of the green ticks indicate the position angle of the linear polarization plane and the tick length is proportional to the radiation flux that is linearly polarized.

simulations and model fitting to the observational broadband SED data). Notice that in the next section different authors use different prescriptions for electron temperatures in their works; hence, the same model may have different appearances.

4. Models vs. observations

The models are matched with observational data by: (1) fitting the synthetic broadband (radio-X-ray) spectral energy distribution to the fluxes observed at various bands (often using non-simultaneous observational data); (2) modeling radio images at millimeter and radio wavelengths, and creating synthetic interferometric data such as visibility amplitudes and visibility closure phases (defined as visibility phase summed over a triangle of interferometric baselines). GRMHD model images can be now compared to a few Very Long Baseline Interferometric (VLBI) data sets of visibility amplitudes at λ=1.3mm (Doeleman *et al.* 2008; Johnson *et al.* 2015) and non-zero closure phases at λ =1.3 and 3.5 mm that indicate the asymmetry in the structure of the source (Fish *et al.* 2016; Ortiz-León *et al.* 2016; Brinkerink *et al.* 2016). Models should also reproduce the linear polarization and circular polarizations levels measured in Sgr A* at different wavelengths using mostly non-VLBI observations (for list of measurements see Table 1 in Shcherbakov *et al.* 2012).

4.1. *Global parameters of the GRMHD simulations*

Table 1 lists various GRMHD simulations that were scaled to the Sgr A* black hole and fitted to the existing data. Different types of models are explored with various values of the black hole spin and various initial magnetic field topologies. Authors also use different observational data sets to fit their models.

The accretion rate onto the black hole is $\dot{M} \approx few \times 10^{-8}\,\mathrm{M_\odot yr^{-1}}$, almost independently of a model used, and we observe the source rather edge-on ($i > 45$ deg). Notice that fitting these models to observational data give significantly different constraints on e.g. a black hole spin parameter. The table also lists two semi-analytical models of jets and advection dominated accretion flow models (Markoff *et al.* 2007;Broderick *et al.* 2016),

https://doi.org/10.1017/S174392131601259X Published online by Cambridge University Press

Model type	a_* range	$B_{t=0}$ loop#	e^-_{disk} $\frac{T_p}{T_e}$	e^-_{jet}	$\|V\|$	ϕ	LP CP	SED	a_* fit	$\dot{M}$ [$M_\odot$/yr]	i [°]	PA [°]	ref.
SANE 2D	0-0.97	1	1	$\frac{T_p}{T_e}=1$	✓	-	✗	✓	$\leqslant 0.88$	$\sim 10^{-9}$	$\geqslant 35$	-	(1)
SANE2D	0-0.98	1	3	$\frac{T_p}{T_e}=3$	✓	-	✗	✓	0.94	1×10^{-9}	85	-	(2)
SANE3D	0.9	1	3	$\frac{T_p}{T_e}=3$	✓	-	✗	✗	-	5×10^{-9}	50	-23	(3)
SANE3D	0-0.98	N	15-20	-	✓	-	✓	✗	0.5	4×10^{-8}	75	115	(4)
tilt15,30°	0.94	1	3	-	✓	-	✗	✓	-	-	-	-	(5)
tilt15°	0.5	1	1	-	✓	-	✗	✗	-	1.8×10^{-8}	40	-81	(6)
SANE2D	0-0.9	1,4	1,3,10	-	✗	-	✗	✓	0.8	1×10^{-9}	-	-	(7)
SANE3D	0.94	1	20	$\Theta_e=20$	✓	-	✗	✓	-	4×10^{-8}	60	-	(8)
SANE3D	0.7,0.9	N	100	$\Theta_e=30$	✓	-	✗	✓	0.9	-	60	140	(9)
MAD3D	0,0.7,0.9	1	1300	$\frac{T_p}{T_e}=316$	✓	-	✗	✓	0.9	-	60	160	(9)
SANE3D	0.92	1	?	$\Theta_e=100$	✓	-	✓	✗	-	2×10^{-8}	126	-	(10)
SANE3D	0.94	2	?	$\Theta_e=50$	✓	-	✓	✗	-	4×10^{-8}	98	-	(10)
MAD3D	0.94	1	?	$\Theta_e=35$	✓	-	✓	✗	-	5×10^{-9}	140	-	(10)
ADAF	0-0.998	-	PL	-	✓	✓	✓	✓	0.1	-	60	156	(11)
JET	-	-	-	PL	✓[1]	✗	✗	✓	-	-	$\geqslant 75$	105	(12)

Table 1. List of recent GRMHD simulations of Sgr A*. First five columns show: model ID, explored range of black hole spins, assumed initial magnetic field configuration, prescription for electron temperatures in the accretion disk, prescription for electron temperatures in the jet. Here PL stands for "power-law" distribution function. Next four columns list which data sets where used to test a model. $|V|$ indicates fit to the visibility amplitudes measured at 1.3mm by Doeleman *et al.* 2008. ϕ is the fit to visibility closure phases at 1.3mm published recently by Fish *et al.* 2016 ([1]fit to 7mm visibility (closure) amplitudes and phases). Here LP and CP stand for level of linear and circular polarization. SED stands for fitting model to spectral energy distribution data from radio to X-rays. Last five columns list the best values of free parameters of the model that fit the observational data best. Rigthmost column references: (1) Noble *et al.* 2007; (2) Mościbrodzka *et al.* 2009; (3) Dexter *et al.* 2010; (4) Shcherbakov *et al.* 2012; (5) Shiokawa 2012; (6) Dexter & Fragile 2013; (7) Drappeau *et al.* 2013; (8) Mościbrodzka *et al.* 2014; (9) Chan *et al.* 2015b; (10) Gold *et al.* 2016; (11) Broderick *et al.* 2016; (12) Markoff *et al.* 2007

which also give different constrains on the model orientation or the black hole spin (in case of ADAF).

Models with radiative jets naturally explain a phenomena such as the radiation spectrum shape. However, as already shown in the earlier work by Özel *et al.* 2000, and more recently by Broderick *et al.* 2016 including non-thermal population of particles in the accretion disk would also produce the flat radio spectrum. Hence, radiative disk models are not yet ruled out.

4.2. *Models for variability at mm wavelengths and NIR/X-ray flares*

The GRMHD simulations are inherently time-dependent. One could test them by comparing the characteristics of the synthetic light curves to the observed ones. This was addressed in detail only in a few publications.

Based on SANE models, Dexter *et al.* (2009) and Dexter *et al.* (2010), under assumption of a constant $T_\mathrm{p}/T_\mathrm{e}$, find that the model light curves show flaring events of 2–3.5 hr duration with about 50% flux modulation at millimeter wavelengths. In these models, the variability is produced by the magnetic turbulence in the inner radii of the accretion flow. The model predictions of the flux modulations are in agreement with the observations of Sgr A* (Dexter *et al.* 2014 and references therein). Dolence *et al.* 2012 discusses variability of SANE models with constant $T_\mathrm{p}/T_\mathrm{e}=3$ at NIR and X-ray bands, and finds quasi-periodic oscillations (QPOs) in the light curves (caused by the inward propagation of magnetic filaments inside the innermost stable circular orbit). Notice that QPOs are

https://doi.org/10.1017/S174392131601259X Published online by Cambridge University Press

not yet found observationally in NIR (Do *et al.* 2009). The SANE models also do not naturally explain the strong NIR and X-ray flares observed in Sgr A* daily.

Dexter & Fragile (2013), with assumption of constant temperature ratio $T_{\rm p}/T_{\rm e} = 1, 3, 5, 20$, modeled the millimeter and NIR emissions of Sgr A* using the tilted disks (see Table 1, also studied in Shiokawa 2012). Tilted disks produce standing shocks in which matter has higher temperatures. The electrons in these regions can naturally reproduce the observed NIR flux and the millimeter/NIR spectral index.

The various types of variability, found in the GRMHD simulations with new prescriptions for electrons temperatures (similar to that expressed by Eq. 3.1), have been recently studied by Chan *et al.* (2015a) (see also the article by C.-K. Chan in this proceeding). They found that their SANE models, in contrast to MAD models, are consistent with the observed millimeter flux variations. Interestingly, their SANE simulations can explain the observed NIR flares (with no X-ray counterparts). The authors suggest that such NIR flares could arise from a combination of short-lived magnetic flux tubes and strong-field gravitational lensing near the horizon.

Neither of the presented models explains the strong X-ray flares observed in Sgr A*. This most likely indicates that additional physics has to be incorporated into the simulations. It has been suggested that the X-ray flares observed in Sgr A* are a result of a sudden acceleration of particles in the inner regions of accretion flow (see early work by Özel *et al.* 2000). For the most recent progress on particle acceleration in GRMHD models see Ball *et al.* (2016).

5. Future studies

Various models of Sgr A* are explored in the community. Extended GRMHD simulations of Sgr A*, such as presented in Ressler *et al.* (2015), are now naturally producing jets that are hotter than disks. While electron temperatures in GRMHD models are now computed with a better confidence, the electrons might not have a purely thermal distribution function. The details of the electron acceleration in GRMHD simulations remain spatially and temporarily unresolved. However, the electron acceleration can be addressed in an approximate manner in which the acceleration of particles occurs in the fluid frame depending on local plasma properties (e.g., Ball *et al.* 2016 and references therein).

There remain several other issues that should be addressed in future models: the structure of accretion flow and magnetic fields at large scales (100–10000 $GM_{\rm BH}/c^2$ from the black hole) which possibly affects the observed position angle of linear polarization; the connection between the large scale plasma motions to matter inflows near the black hole event horizon; dynamics and appearance of accretion disks and jets in non-Kerr metrics. See Goddi *et al.* (2016) for more details.

Acknowledgements

I acknowledge support from the ERC Synergy Grant "BlackHoleCam - Imaging the Event Horizon of Black Holes" (Grant 610058).

References

Abramowicz, M. A. & Fragile, P. C. 2013, Living Reviews in Relativity, 16
Balbus, S. A. & Hawley, J. F. 1998, Reviews of Modern Physics, 70, 1
Ball, D., Özel, F., Psaltis, D., & Chan, C.-k. 2016, *ApJ*, 826, 77
Beckwith, K., Hawley, J. F., & Krolik, J. H. 2008, *ApJ*, 678, 1180

Bower, G. C., Markoff, S., Brunthaler, A., *et al.* 2014, *ApJ*, 790, 1
Brinkerink, C. D., Müller, C., Falcke, H., *et al.* 2016, *MNRAS*, 462, 1382
Broderick, A. E., Fish, V. L., Johnson, M. D., *et al.* 2016, *ApJ*, 820, 137
Chan, C.-k., Psaltis, D., Özel, F., *et al.* 2015a, *ApJ*, 812, 103
Chan, C.-K., Psaltis, D., Özel, F., Narayan, R., & Sądowski, A. 2015b, *ApJ*, 799, 1
Dexter, J., Agol, E., & Fragile, P. C. 2009, *ApJ*, 703, L142
Dexter, J., Agol, E., Fragile, P. C., & McKinney, J. C. 2010, *ApJ*, 717, 1092
Dexter, J. & Fragile, P. C. 2013, *MNRAS*, 432, 2252
Dexter, J., Kelly, B., Bower, G. C., *et al.* 2014, *MNRAS*, 442, 2797
Dibi, S., Drappeau, S., Fragile, P. C., Markoff, S., & Dexter, J. 2012, *MNRAS*, 426, 1928
Do, T., Ghez, A. M., Morris, M. R., *et al.* 2009, *ApJ*, 691, 1021
Doeleman, S. S., Weintroub, J., Rogers, A. E. E., *et al.* 2008, *Nature*, 455, 78
Dolence, J. C., Gammie, C. F., Shiokawa, H., & Noble, S. C. 2012, *ApJ*, 746, L10
Drappeau, S., Dibi, S., Dexter, J., Markoff, S., & Fragile, P. C. 2013, *MNRAS*, 431, 2872
Falcke, H., Mannheim, K., & Biermann, P. L. 1993, *A&A*, 278, L1
Falcke, H. & Markoff, S. 2000, *A&A*, 362, 113
Fish, V. L., Johnson, M. D., Doeleman, S. S., *et al.* 2016, *ApJ*, 820, 90
Fraga-Encinas, R., Mościbrodzka, M., Brinkerink, C., & Falcke, H. 2016, *A&A*, 588, A57
Fragile, P. C., Blaes, O. M., Anninos, P., & Salmonson, J. D. 2007, *ApJ*, 668, 417
Goddi, C., Falcke, H., Kramer, M., *et al.* 2016, ArXiv e-prints
Gold, R., McKinney, J. C., Johnson, M. D., & Doeleman, S. S. 2016, ArXiv e-prints
Howes, G. G. 2011, *ApJ*, 738, 40
Ichimaru, S. 1977, *ApJ*, 214, 840
Johnson, M. D., Fish, V. L., Doeleman, S. S., *et al.* 2015, Science, 350, 1242
Markoff, S., Bower, G. C., & Falcke, H. 2007, *MNRAS*, 379, 1519
Marrone, D. P., Moran, J. M., Zhao, J.-H., & Rao, R. 2007, *ApJ*, 654, L57
McKinney, J. C. & Gammie, C. F. 2004, *ApJ*, 611, 977
McKinney, J. C., Tchekhovskoy, A., & Blandford, R. D. 2012, *MNRAS*, 423, 3083
Mościbrodzka, M. & Falcke, H. 2013, *A&A*, 559, L3
Mościbrodzka, M., Falcke, H., Shiokawa, H., & Gammie, C. F. 2014, *A&A*, 570, A7
Mościbrodzka, M., Gammie, C. F., Dolence, J. C., Shiokawa, H., & Leung, P. K. 2009, *ApJ*, 706, 497
Narayan, R., Igumenshchev, I. V., & Abramowicz, M. A. 2003, *PASJ*, 55, L69
Narayan, R., Mahadevan, R., Grindlay, J. E., Popham, R. G., & Gammie, C. 1998, *ApJ*, 492, 554
Noble, S. C., Leung, P. K., Gammie, C. F., & Book, L. G. 2007, Classical and Quantum Gravity, 24, S259
Ortiz-León, G. N., Johnson, M. D., Doeleman, S. S., *et al.* 2016, *ApJ*, 824, 40
Özel, F., Psaltis, D., & Narayan, R. 2000, *ApJ*, 541, 234
Quataert, E. & Narayan, R. 1999, *ApJ*, 520, 298
Ressler, S. M., Tchekhovskoy, A., Quataert, E., Chandra, M., & Gammie, C. F. 2015, *MNRAS*, 454, 1848
Sadowski, A., Wielgus, M., Narayan, R., Abarca, D., & McKinney, J. C. 2016, ArXiv e-prints
Shcherbakov, R. V., Penna, R. F., & McKinney, J. C. 2012, *ApJ*, 755, 133
Tchekhovskoy, A., Narayan, R., & McKinney, J. C. 2011, *MNRAS*, 418, L79
Yuan, F., Markoff, S., & Falcke, H. 2002, *A&A*, 383, 854
Yuan, F. & Narayan, R. 2014, *ARA&A*, 52, 529

https://doi.org/10.1017/S174392131601259X Published online by Cambridge University Press